# Chapter 2
# Mathematical Modeling of Physiological Systems

**Thomas Heldt, George C. Verghese, and Roger G. Mark**

**Abstract** Although mathematical modeling has a long and very rich tradition in physiology, the recent explosion of biological, biomedical, and clinical data from the cellular level all the way to the organismic level promises to require a renewed emphasis on *computational physiology*, to enable integration and analysis of vast amounts of life-science data. In this introductory chapter, we touch upon four modeling-related themes that are central to a computational approach to physiology, namely simulation, exploration of hypotheses, parameter estimation, and model-order reduction. In illustrating these themes, we will make reference to the work of others contained in this volume, but will also give examples from our own work on cardiovascular modeling at the systems-physiology level.

## 2.1 Introduction

Mathematical modeling has a long and very rich history in physiology. Otto Frank's mathematical analysis of the arterial pulse, for example, dates back to the late nineteenth century [12]. Similar mathematical approaches to understanding the mechanical properties of the circulation have continued over the ensuing decades, as recently reviewed by Bunberg and colleagues [5]. By the middle of the last century,

T. Heldt (✉) · G.C. Verghese
Computational Physiology and Clinical Inference Group, Research Laboratory of Electronics, Massachusetts Institute of Technology, 10-140L, 77 Massachusetts Avenue, Cambridge, MA 02139, USA
e-mail: thomas@mit.edu; verghese@mit.edu

R.G. Mark
Laboratory for Computational Physiology, Harvard-MIT Division of Health Sciences and Technology, Massachusetts Institute of Technology, E25-505, 77 Massachusetts Avenue, Cambridge, MA 02139, USA
e-mail: rgmark@mit.edu

J.J. Batzel et al. (eds.), *Mathematical Modeling and Validation in Physiology*, Lecture Notes in Mathematics 2064, DOI 10.1007/978-3-642-32882-4_2,

Hodgkin and Huxley had published their seminal work on neuronal action-potential initiation and propagation [25], from which models of cardiac electrophysiology readily emerged and proliferated [33]. To harness the emergent power of first analog and later digital computers, mathematical modeling in physiology soon shifted from analytical approaches to computational implementations of governing equations and their simulation. This development allowed for an increase in the scale of the problems addressed and analyzed. In the late 1960s, Arthur Guyton and his associates, for example, developed an elaborate model of fluid-electrolyte balance that still impresses today for the breadth of the physiology it represents [16].

Since the days of Guyton's initial work, the widespread availability of relatively low-cost, high-performance computer power and storage capacity has enabled physiological modeling to move from dedicated—and oftentimes single-purpose—computers to the researcher's desktop, as even small-scale computer clusters can be assembled at comparatively little expense. The technological advancements in computer power and digital storage media have also permitted increasingly copious amounts of biological, biomedical, and even clinical data to be collected and archived as part of specific research projects or during routine clinical management of patients. Our ability to collect, store, and archive large volumes of data from all biological time and length scales is therefore no longer a rate-limiting step in scientific or clinical endeavors. Ever more pressing, however, is the concomitant need to link characteristics of the observed data streams mechanistically to the properties of the system under investigation and thereby turn—possibly in real-time as required by some clinical applications [23]—otherwise overwhelming amounts of biomedical data into an improved understanding of the biological systems themselves. This link is the mechanistic, mathematical and computational modeling of biological systems at all physiological length and time scales, as envisioned by the Physiome project [3, 8, 26].

Mechanistic mathematical models reflect our present-level understanding of the functional interactions that determine the overall behavior of the system under investigation. By casting our knowledge of physiology in the framework of dynamical systems (deterministic or stochastic), we enable precise quantitative predictions to be made and to be compared against results from suitably chosen experiments. Mechanistic mathematical models often allow us to probe a system in much greater detail than is possible in experimental studies and can therefore help establish the cause of a particular observation [22]. When fully integrated into a scientific program, mathematical models and experiments are highly synergistic, in that the existence of one greatly enhances the value of the other: models depend on experiments for specification and refinement of parameter values, but they also illuminate experimental observations, allow for differentiation between competing scientific hypotheses, and help aid in experimental design [22]. Analyzing models rigorously, through sensitivity analyses, formal model-order reduction, or simple simulations of what-if scenarios also allow for identification of crucial gaps in our knowledge and therefore help motivate the design of novel experiments. Finally, mathematical models serve as important test beds against which estimation and identification algorithms can be evaluated, as the true target values are precisely

known and controllable [20]. It seems therefore that a renewed emphasis on *computational physiology* is not merely a positive development, but an essential step toward increasing our knowledge of living systems in the twenty-first century.

In this chapter, we will touch upon four main themes of mathematical modeling, namely simulation, exploration of hypotheses, parameter estimation, and model-order reduction. In addition to drawing upon our own work to illustrate these application areas, we will point the reader to the work of others, some of which is represented in this volume.

## 2.2 Simulation

Given a chosen model structure and a nominal set of parameter values, a central application of mathematical modeling is the simulation of the modeled system. Closely related to the simulation exercise is the comparison of the simulated model response to experimental data. In the area of respiratory physiology, the contributions by Bruce (Chap. 7) and Duffin (Chap. 8) in this volume are examples of such applications of mathematical modeling. The contributions by Tin and Poon (Chap. 5) and Ottesen and co-workers (Chap. 10) focus on modeling the respiratory control system and the cardiovascular response to orthostatic stress, respectively.

Our own interest in the cardiovascular response to changes in posture led us to develop a detailed lumped-parameter model of the cardiovascular system [17]. The model consists of a 21-compartment representation of the hemodynamic system, shown in Fig. 2.1, coupled to set-point controllers of the arterial baroreflex and the cardiopulmonary reflex, as depicted in Fig. 2.2, that mimic the short-term action of the autonomic nervous system in maintaining arterial and right-atrial pressures constant (blood pressure homeostasis) [17, 22].

In the context of cardiovascular adaptation to orthostatic stress, numerous computational models have been developed over the past 40 years [4, 9–11, 15, 24, 27–29, 31, 32, 34, 35, 38, 39, 41–43, 48, 49, 51]. Their applications range from simulating the physiological response to experiments such as head-up tilt or lower body negative pressure [4, 9, 10, 15, 27–29, 31, 32, 38, 43, 50, 51], to explaining observations seen during or following spaceflight [29, 35, 42, 44, 48, 51]. The spatial and temporal resolutions with which the cardiovascular system has been represented are correspondingly broad. Several studies have been concerned with changes in steady-state values of certain cardiovascular variables [35, 41, 43, 48], others have investigated the system's dynamic behavior over seconds [15, 24, 27, 28, 34], minutes [4, 9, 10], hours [29, 42, 51], days [29, 39, 42], weeks [29], or even months [38]. The spatial representations of cardiovascular physiology range from simple two- to four-compartment representations of the hemodynamic system [4, 15, 31, 32, 48] to quasi-distributed or fully-distributed models of the arterial or venous system [28, 35, 41, 43].

In choosing the appropriate time scale of our model, we were guided by the clinical practice of diagnosing orthostatic hypotension, which is usually based on average values of hemodynamic variables measured a few minutes after the onset

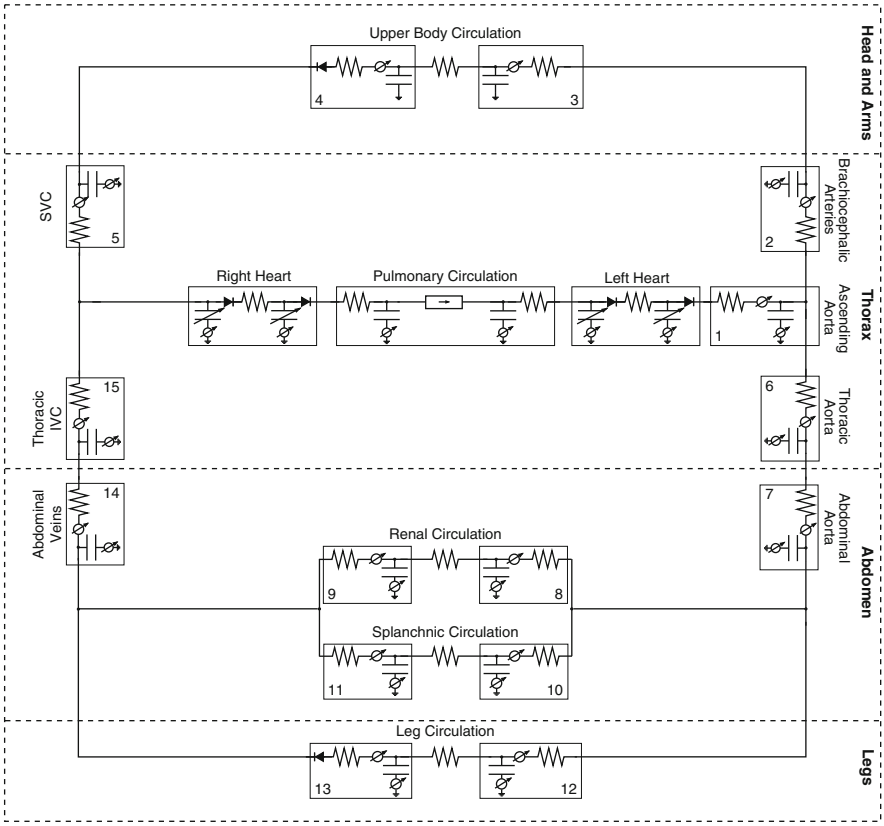


**Fig. 2.1** Circuit representation of the hemodynamic system. *IVC*: inferior vena cava; *SVC*: superior vena cava

of gravitational stress [7]. The spatial resolution of our model was dictated by our desire to represent the prevailing hypotheses of post-spaceflight orthostatic intolerance (see Sect. 2.3). To determine a set of nominal parameter values, we searched the medical literature for appropriate studies on healthy subjects. In cases in which direct measurements could not be found, we estimated nominal parameter values on the basis of physiologically reasonable assumptions [17, 22]. We tested our simulations against a series of experimental observations by implementing a variety of stress tests, such as head-up tilt, supine to standing, lower-body negative pressure, and short-radius centrifugation, all of which are commonly used in clinical or research settings to assess orthostatic tolerance [17, 52].

Figure 2.3 shows simulations (solid lines) of the steady-state changes in mean arterial blood pressure and heart rate in response to head-up tilts to varying angles of elevation [17, 19], along with experimental data taken from Smith and co-workers [40]. (The dashed lines in this and later figures from simulations indicate the 95 % confidence limits of the nominal simulation on the basis of representative population simulations [18].) In Fig. 2.4, we show the dynamic

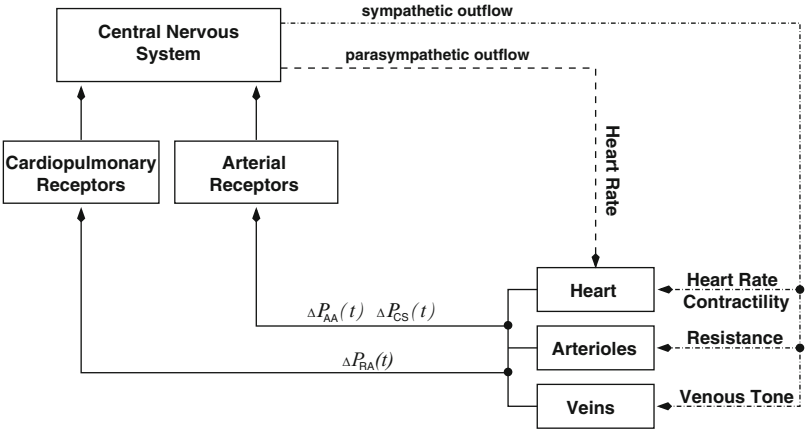


**Fig. 2.2** Schematic representation of the cardiovascular control model. $\Delta P_{AA}(t)$, $\Delta P_{CS}(t)$, $\Delta P_{RA}(t)$: aortic arch, carotid sinus, and right atrial transmural pressures, respectively

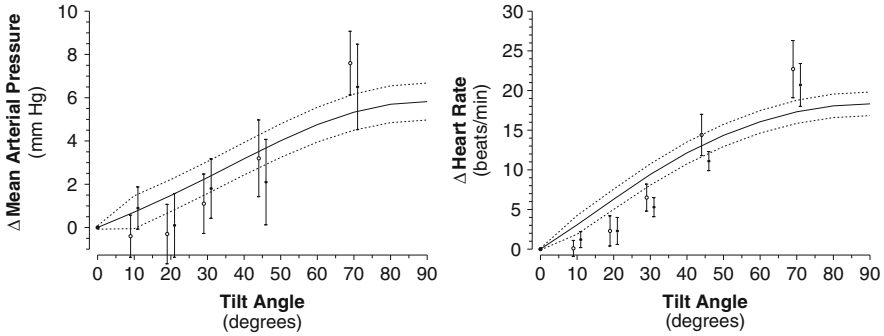


**Fig. 2.3** Simulated steady-state changes (*solid lines*) and 95 % confidence intervals (*dashed lines*) in mean arterial pressure (*left*) and heart rate (*right*), in response to head-up tilt maneuvers to different angles of elevation. Data for young subjects (*open circles*) and older subjects (*filled circles*) from Smith et al. [40]

responses of measured mean arterial blood pressure and heart rate (lower panels) and the respective simulated responses (upper panels) to a rapid head-up tilt experiment [17,21]. Figure 2.5 shows the dynamic behavior of the same variables in response to standing up from the supine position. The simulations of Figs. 2.3–2.5 were all performed with the same set of nominal parameter values, and the same population distribution of parameter values.

Similar dynamic responses in arterial blood pressure and heart rate to orthostatic challenges have been reported by van Heusden [24] and Olufsen et al. [34], and are reported by Ottesen et al. in this volume (Chap. 11) for the transition from sitting to standing.

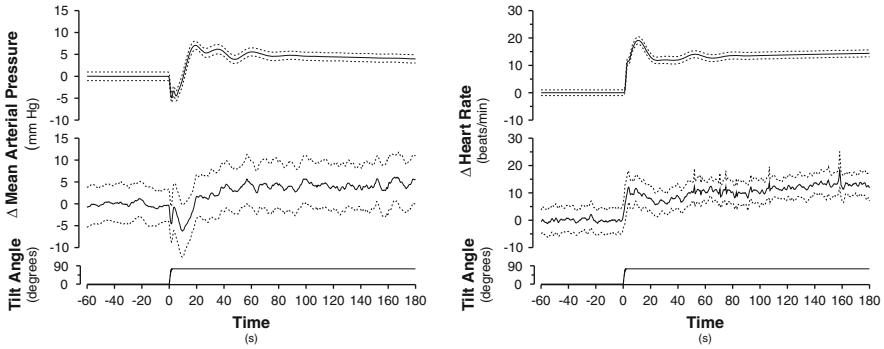


**Fig. 2.4** Dynamic responses in mean arterial pressure (*left*) and heart rate (*right*) to a sudden head-up tilt maneuver. *Bottom panels* show experimental recordings [21]; *upper panels* show simulated responses [17]

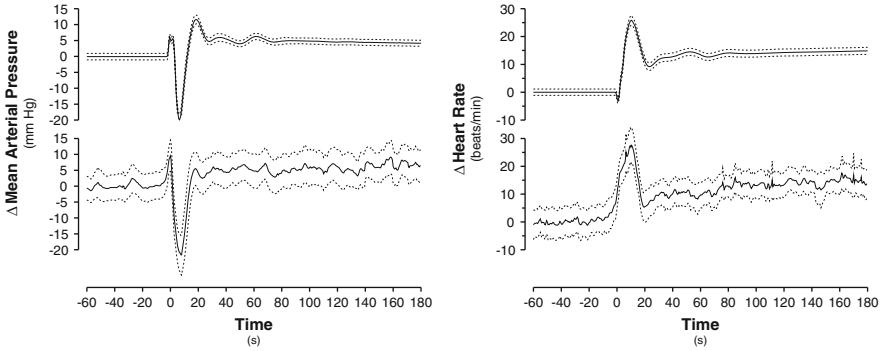


**Fig. 2.5** Dynamic responses (*solid lines*) and 95 % confidence intervals (*dashed lines*) in mean arterial pressure (*left*) and heart rate (*right*) to standing up. *Bottom panels* show recordings [21]; *upper panels* show simulated responses [17]

Once a particular model structure has been chosen and simulations have been calibrated and validated against suitable sets of experimental data, the ensuing scientific step usually involves exploration of particular physiological hypotheses, or detailed sensitivity analyses as pursued by Banks (Chap. 3) or Ottesen (Chap. 10) in this volume.

## 2.3 Exploration of Hypotheses

Using the model of the previous section, we were interested in gaining insight into the cardiovascular system's failure to adapt to the upright posture following spaceflight. By simulating the system-level hemodynamic response to a tilt or a

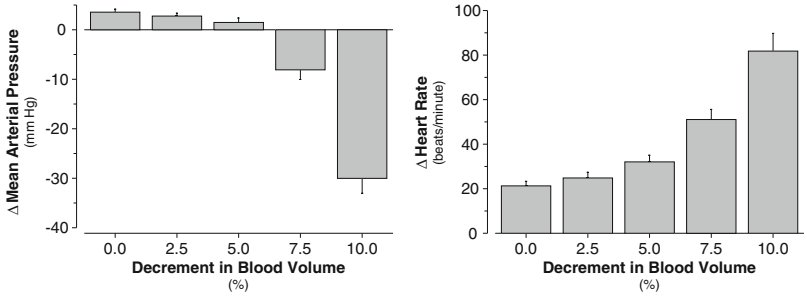


**Fig. 2.6** Mean arterial pressure and heart rate changes induced by head-up tilt to 75°. Dependence on volume status. Mean response ± SE based on 20 simulations

stand test under varying parameter profiles, we sought to identify which of the prevailing physiological hypotheses lead to the system-level hypotension seen in affected astronauts upon assumption of the upright posture. This approach can be viewed as a targeted sensitivity analysis that differs from the more general explorations presented by Banks (Chap. 3), in that the parameters to be varied are selected based on *a priori* physiological considerations. Furthermore, the parameter values will be subjected to larger perturbations than in the more local analysis of Chap. 3.

In our analysis, we choose to include those parameters that have been implicated in contributing to the post-flight orthostatic intolerance phenomenon [17]. Our analysis therefore includes total blood volume, the venous compliance of the legs, the end-diastolic compliance of the right ventricle, and the static gain values (both arterial and cardiopulmonary) of arteriolar resistance and venous tone. We assess the impact of parameter perturbations by analyzing the changes they induce in the mean arterial pressure and heart rate responses to a 75° head-up tilt. In particular, we seek to answer which of the parameters included in the analysis has the greatest impact on mean arterial pressure and heart rate.

We address this question by repeatedly simulating tilt experiments while varying each of the parameters by a certain percentage of their nominal values. In Fig. 2.6, we report the changes in mean arterial pressure and heart rate from their respective supine baselines in response to a 4 min head-up tilt to 75° for varying levels of total blood volume. We note that head-up tilt usually results in a slight *increase* in mean arterial pressure measured at heart level, with a concomitant increase in heart rate. Figure 2.6 reflects this fact as the baseline simulation (0 % decrement in total blood volume, or 70 ml/kg of body weight) shows an increase in mean arterial pressure of about 4 mm Hg and an increase of approximately 20 beats/min in heart rate. As blood volume is progressive reduced, the gentle rise in mean arterial pressure is diminished, but generally maintained up to volume decrements of 5 %. Beyond that, the system fails to maintain mean arterial pressure despite incrementally larger increases in heart rate. The reason for this behavior becomes

clear when we consider blood pooling in the dependent vasculature during tilt as a function of hydration status. With increasing degree of hypovolemia, the amount of blood volume pooled in the lower extremities becomes an increasingly larger fraction of distending volume. It therefore becomes progressively more difficult for the cardiovascular system to maintain right atrial pressure, and thus cardiac output, during head-up tilt.

In Fig. 2.7, we display the results of the same analysis for the venous compliance of the legs, the right-ventricular end-diastolic compliance, and the arterial and venous tone feedback gain values (top to bottom). Each of the simulations underlying Fig. 2.7 starts with the same baseline blood volume, which, for future reference, we term the euvolemic baseline state. When comparing the results in Fig. 2.7 with the volume-loss results in Fig. 2.6, it is obvious that deleterious changes in any of the parameters shown in Fig. 2.7 only marginally impact the hemodynamic response to tilt if the volume status if euvolemic. In other words, in the absence of hypovolemia, the body can tolerate significant detrimental changes in any of the other parameters without developing a seriously compromised hemodynamic response to tilt.

Next, we demonstrate that this behavior can change drastically if the baseline volume status is changed. In Fig. 2.8, we vary the four parameters of Fig. 2.7 by the same fractional changes, yet their variation is superimposed on a baseline state that is 5 % hypovolemic compared to the euvolemic baseline states of Figs. 2.6 and 2.7. The results demonstrate that against the backdrop of an otherwise benign reduction in total blood volume, even modest 5 % to 10 % detrimental changes in each of the parameters can significantly impact the hemodynamic response to tilt.

The results of the simulations show that the level of hydration has by far the greatest impact on blood pressure homeostasis during tilt. Furthermore, the impact of changes in other parameters varies significantly with the level of hydration. In the euvolemic state, changes in the four parameters considered in Figs. 2.7 and 2.8 have similar effects on the mean arterial pressure and heart rate responses. In the hypovolemic case, changes in venous tone seem to impact the hemodynamic response to tilt more when compared with the same fractional changes in the other parameters, yet all of the parameters considered significantly influence the heart rate and mean arterial pressure responses to head-up tilt.

The simulations presented in this section demonstrate the importance of blood volume in maintaining mean arterial pressure during orthostatic stress. Changes in the other parameters included in this analysis are largely inconsequential if total blood volume is maintained near euvolemic levels (70 ml/kg). However, if the baseline state is hypovolemic, even relatively modest changes in these parameters can aggravate the cardiovascular system's failure to adapt properly to the upright posture. Reductions in both the arterial resistance gains and the venous tone gains affect mean arterial pressure most; impairment of the venous tone feedback, however, has a stronger effect when the same fractional decrements in the nominal values are considered.

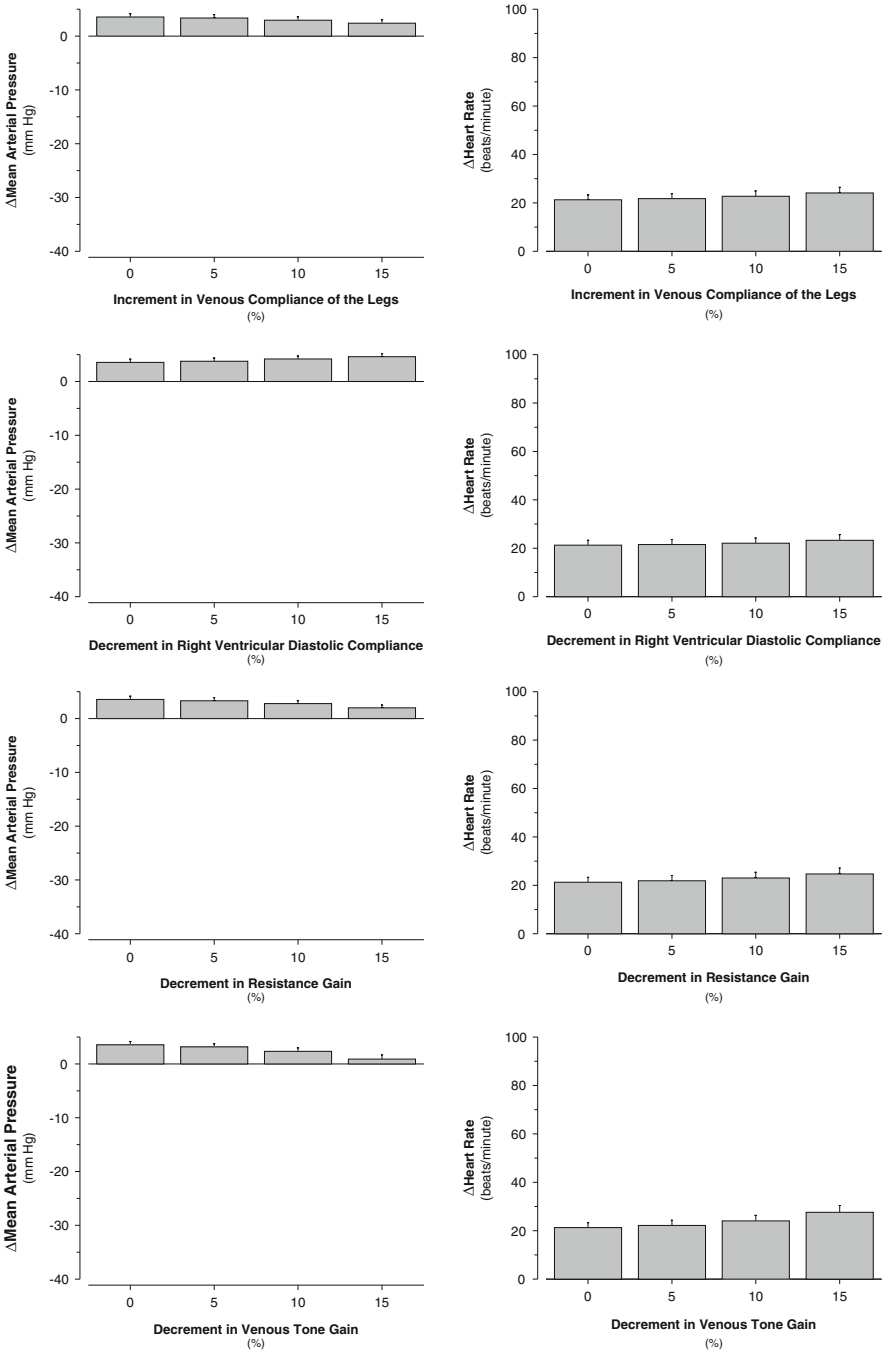


**Fig. 2.7** Mean arterial pressure and heart rate changes in response to a 75° head-up tilt under varying parametric conditions. Baseline volume status is euvolemic. Mean response ± SE based on 20 simulations

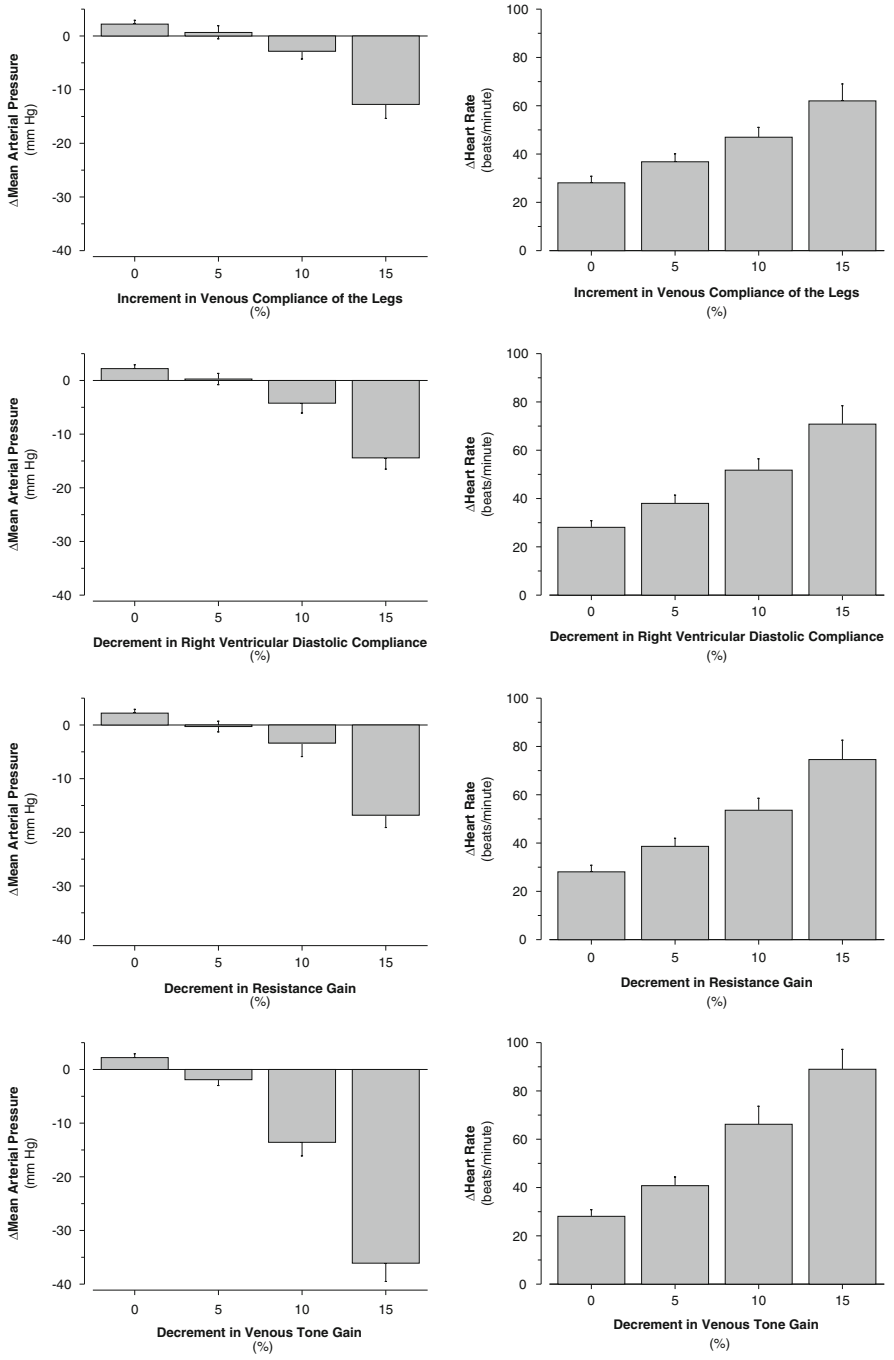


**Fig. 2.8** Mean arterial pressure and heart rate changes in response to a 75° head-up tilt under varying parametric conditions. Baseline volume status is 5 % hypovolemic. Mean response ± SE based on 20 simulations

Reductions in total blood volume in returning astronauts have been well established, though the magnitude of the hypovolemia is highly variable. The work by Waters and co-workers suggest a mean overall reduction of about 6 % in male pre-syncopal astronauts [47]. Our simulations give credence to the view that hypovolemia can be the principal mechanism of post-spaceflight orthostatic intolerance, yet at an average level of 6 % might not be solely responsible for the clinical picture of the syndrome. Of particular importance, therefore, are perturbations to the $\alpha$-sympathetically mediated reflex pathways of arteriolar resistance and venous tone, both of which depend on the peripheral neurotransmitter norepinephrine. Ramsdell et al. demonstrated that an exogenous $\alpha$-adrenergic agonist, when given to subjects undergoing orthostatic stress testing at the conclusion of a prolonged bedrest protocol, significantly reduces the incidence of syncope or pre-syncopal symptoms [37]. Furthermore, Meck et al. showed that those astronauts who become pre-syncopal on landing day fail to mount a significant vasoconstrictor response due to an inappropriately low release of norepinephrine in the upright posture [30]. Finally, Platts and co-workers demonstrated that the same $\alpha$-agonist used by Ramsdell was beneficial in alleviating post-spaceflight orthostatic intolerance in a female astronaut who had a prior history of orthostatic hypotension after previous missions [36]. In the context of our model, failure to release norepinephrine at the smooth muscle synapses is interpreted as a reduction in the gain from arterial blood pressure and right atrial pressure to venous tone and arterial resistance.

Together, these experimental findings corroborate the results from our simulation studies, namely that a critical combination of mechanisms might have to be invoked to explain the phenomenon of post-spaceflight orthostatic intolerance, and that apart from hypovolemia, detrimental changes to the feedback pathway to vascular smooth muscle (venous tone and arteriolar resistance) play a dominant role.

## 2.4 Model Identification

Mechanistic physiological models tend to have relatively high spatial and temporal resolution for their ultimate application and therefore involve large numbers of parameters and exhibit rich dynamic behavior, spanning several time scales. Such a modeling approach, in which models are built from detailed analysis of the underlying physiological or biological processes, is commonly referred to as *forward modeling*. Often, the purpose of modeling is to use the resultant model in conjunction with experimental data to estimate the values of some model parameters. Such a strategy falls under the general umbrella of *inverse methods* in which attributes of a system are estimated based on measurements that are only indirectly related to these attributes [46]. The link between the attributes and the data is the mathematical model.

In such parameter estimation problems, the parameters of a model are tuned such that a measure of error between the model output and a corresponding set of observations is minimized. Methods for solving this minimization problem depend

quite naturally on the error criterion and on the structure of the chosen model. Furthermore, the quality of the resultant parameter estimates also depends on the fidelity of the available data.

In this volume, the contributions by Attarian and co-workers (Chap. 4), Banks and co-workers (Chap. 3), Ottesen et al. (Chap. 10), and Hartung and Turi (Chap. 6) focus on specific aspects of inverse modeling. Attarian focuses on the topic of Kalman filtering for both parameter and state estimation, while Banks' chapter provides an overview of statistical methods to address the parameter estimation problem, particularly the issue of subset selection which we will touch upon later in this section, too. Ottesen highlights the application of parameter estimation methods to the clinical problem of estimating cerebrovascular variables. Hartung and Turi apply parameter estimation to the identification of the respiratory control system. The contribution by Bruce (Chap. 7) similarly focuses on identifying respiratory control loops.

Our own interest in parameter estimation initially developed in the context of cardiovascular applications, where the number of signals available from physiological experiments are usually small in number. Quite often, the only signals recorded are beat-to-beat mean arterial pressure and heart rate during rest or a particular stress-test intervention to challenge the cardiovascular system. The models developed, however, can be quite detailed in their representation of cardiovascular physiology. Thus a disparity exists between the high resolution and rich dynamic behavior of the model and the low resolution and limited dynamic behavior of the measurements. In the parameter estimation setting, this disparity leads to a very sensitive—or *ill-conditioned*—estimation problem, in which small changes to the input data can lead to very large and obviously undesirable changes to the resultant parameter estimates. Since treatment of ill-conditioning is not commonly found in the physiological modeling literature, we present in some detail one possible approach, namely subset selection, to overcome this problem. Our exposition in the remainder of this section is largely based on [17].

### *2.4.1 Non-linear Least-Squares Estimation*

If the model outputs are linear functions of the model parameters, and if the error measure is chosen to be the sum of squares of the prediction error on each output, the resultant minimization problem is the well-known *linear least squares problem*. If the model output is a *non-linear* function of the parameters, the minimization problem is usually solved iteratively through a sequence of linear least squares problems that involve the gradient or higher-order derivatives of the cost function.

Let $\Phi(\hat{\mathbf{y}}(\theta), \mathbf{y})$ denote a non-negative measure of error, or cost function, between model output $\hat{\mathbf{y}}(\theta) \in R^n$ and experimental data $\mathbf{y} \in R^n$. Through the model output, $\Phi$ is an implicit function of the vector of model parameters $\theta \in R^m$ and can therefore be considered a function from $R^m$ to the non-negative real line, $\Phi = \Phi(\theta) : R^m \to R^+ \cup \{0\}$, for a given experimental data set. Since we aim to

minimize this measure of error iteratively, we seek a computational scheme that provides us with a new parameter vector $\theta_1$ such that $\Phi(\theta_1) < \Phi(\theta_0)$ given an initial best guess $\theta_0$. Once such a $\theta_1$ has been identified, it can assume the role of $\theta_0$, and we can repeat the computational scheme in an effort to reduce the measure of error even further.

Let us assume that a second-order Taylor series approximation $\Psi$ of $\Phi(\theta)$ is a good approximation of the local behavior of the cost function for small perturbations $\Delta\theta = \theta - \theta_0$ around the initial parameter estimate. [$\Psi(\theta)$ is the best second-order approximation to the surface defined by $\Phi(\theta)$ around $\theta_0$.] $\Psi(\theta)$ is given by

$$\Psi(\theta) = \Phi(\theta_0) + \left[\frac{\partial \Phi}{\partial \theta}\right]_{\theta_0} \Delta\theta + \frac{1}{2}\ \Delta\theta^{\mathsf{T}} \left[\frac{\partial^2 \Phi}{\partial \theta^2}\right]_{\theta_0} \Delta\theta,$$

where $[\partial\Phi/\partial\theta]_{\theta_0}$ and $\left[\partial^2\Phi/\partial\theta^2\right]_{\theta_0}$ are the appropriate matrices of the first- and second-order derivatives evaluated at the current best guess of the parameter vector as indicated by the subscript $\theta_0$. To find its minimum, we equate to zero the gradient of $\Psi(\theta)$:

$$\frac{\partial}{\partial \theta}\Psi(\theta) = \left[\frac{\partial \Phi}{\partial \theta}\right]_{\theta_0} + \left[\frac{\partial^2 \Phi}{\partial \theta^2}\right]_{\theta_0} \Delta\theta = 0,$$

which leads to the following condition for the stationary point $\theta_1$:

$$\left[\frac{\partial^2 \Phi}{\partial \theta^2}\right]_{\theta_0} (\theta_1 - \theta_0) = -\left[\frac{\partial \Phi}{\partial \theta}\right]_{\theta_0}.$$

If the inverse of the second-order derivative matrix exists, the stationary point is given by:

$$\theta_1 = \theta_0 - \left[\frac{\partial^2 \Phi}{\partial \theta^2}\right]_{\theta_0}^{-1} \cdot \left[\frac{\partial \Phi}{\partial \theta}\right]_{\theta_0}. \tag{2.1}$$

It can be shown that $\Phi(\theta_1) < \Phi(\theta_0)$ if and only if the matrix of second-order derivatives is positive definite [2].

Note that we have not yet specified the cost function $\Phi$. The results obtained so far only require it to be twice differentiable. Let us assume now that we are aiming to minimize the square of the residual error $\mathbf{r}(\theta) = \hat{\mathbf{y}}(\theta) - \mathbf{y}$ between model output and actual measurements, that is

$$\Phi(\theta) = \frac{1}{2} \cdot \|\mathbf{r}(\theta)\|^2 = \frac{1}{2} \cdot \|\hat{\mathbf{y}}(\theta) - \mathbf{y}\|^2 = \frac{1}{2} \cdot \mathbf{r}^{\mathsf{T}}\mathbf{r} \to \min,$$

where the factor of $1/2$ has been included for convenience, and the superscript $^{\mathsf{T}}$ denotes transposition. The gradient of this cost function is given by:

$$\left[\frac{\partial \Phi}{\partial \theta}\right] = \mathbf{J}^{\mathsf{T}} \cdot \mathbf{r}(\theta) \quad \text{where} \quad \mathrm{J}_{ij} = \frac{\partial r_i(\theta)}{\partial \theta_j} = \frac{\partial \hat{y}_i(\theta)}{\partial \theta_j}.$$

$\mathbf{J} \in R^{n \times m}$ denotes the Jacobian matrix of the error vector with respect to the parameter vector. Similarly, we can compute the elements of the Hessian matrix $\mathbf{H} \in R^{m \times m}$ of second derivatives of the cost function:

$$H_{ij} = \frac{\partial^2 \Phi}{\partial \theta_i \partial \theta_j} = (\mathbf{J}^\mathsf{T}\mathbf{J})_{ij} + \sum_{l=1}^{n} r_l \cdot \frac{\partial^2 r_l}{\partial \theta_i \partial \theta_j}. \tag{2.2}$$

Note that for small residuals, the Hessian can be approximated by

$$H_{ij} = \frac{\partial^2 \Phi}{\partial \theta_i \partial \theta_j} \approx (\mathbf{J}^\mathsf{T}\mathbf{J})_{ij}, \tag{2.3}$$

since the second term involves the elements of the vector of residuals directly. This approximation is known as the Gauss–Newton approximation to the Hessian.

Inserting the expressions for the derivatives into Eq. (2.1), we obtain the iterative parameter updates of the Newton method:

$$\mathbf{H} \cdot (\theta_{i+1} - \theta_i) = -\mathbf{J}^\mathsf{T} \cdot \mathbf{r} \tag{2.4}$$

and the Gauss–Newton approximation thereof:

$$\mathbf{J}^\mathsf{T}\mathbf{J} \cdot (\theta_{i+1} - \theta_i) = -\mathbf{J}^\mathsf{T} \cdot \mathbf{r}. \tag{2.5}$$

Let $\mathbf{R}$ denote either the full Hessian $\mathbf{H}$ or its Gauss–Newton approximation $\mathbf{J}^\mathsf{T}\mathbf{J}$. If $\mathbf{R}$ has full column rank, Eqs. (2.4) and (2.5) can be solved exactly or in a least squares sense, depending on whether or not $\mathbf{J}^\mathsf{T} \cdot \mathbf{r}$ is in the column space of $\mathbf{R}$. In either case, however, the solution is unique, and efficient algorithms exist to solve the set of linear equations numerically [14]. If, on the other hand, $\mathbf{R}$ is rank-deficient, then the $m$ columns of $\mathbf{R}$ actually contain less than $m$ linearly independent vectors. As a consequence, $\mathbf{R}$ is semi-definite with at least one of its eigenvalues at zero. The following argument by Burth and co-workers [6] illustrates the problem of a singular matrix $\mathbf{R}$ in the context of parameter estimation. Assume $\mathbf{R}$ has a single eigenvalue at zero with some associated eigenvector $\vartheta$. Within the limits of our second-order approximation, $\vartheta$ can be added to any step direction without affecting the error criterion, since

$$\mathbf{R} \cdot (\theta_{i+1} - \theta_i + \vartheta) = \mathbf{R} \cdot (\theta_{i+1} - \theta_i) + \mathbf{R} \cdot \vartheta = \mathbf{R} \cdot (\theta_{i+1} - \theta_i) = -\mathbf{J}^\mathsf{T} \cdot \mathbf{r}.$$

This implies that we can arbitrarily change parameter values along the direction of $\vartheta$ without affecting the error criterion. Such indeterminacy suggests that the parameters of the model cannot be estimated uniquely from the given measurements; the estimation problem is said to be ill-conditioned.

Frequently, the matrix $\mathbf{R}$ is not exactly rank deficient but quite nearly so, in the sense that the largest eigenvalue is orders of magnitude larger than the smallest

eigenvalue. Closeness to singularity is measured by the condition number $\kappa(\mathbf{R})$ which, for real, symmetric matrices, is given by the ratio of the largest to the smallest eigenvalue.

Burth reviews several related consequences of a large condition number for estimation problems [6]. We simply note here that a hallmark of an ill-conditioned problem is its extreme sensitivity to small perturbations in either the experimental data or the elements of the matrix $\mathbf{R}$. In the following section we discuss subset selection as an approach to overcome this ill-conditioning.

### 2.4.2 Subset Selection

Subset selection aims to determine which parameter axes lie closest to the singular directions of the Hessian matrix [45]. Changes in the corresponding parameters do relatively little to change the fit of the model to the data, and therefore these parameters are hard to estimate reliably. Once these ill-conditioned parameter axes are identified, one can fix the associated parameters at prior values throughout the estimation process, thus improving the conditioning of the resultant reduced-order estimation problem. Fixing values of the ill-conditioned parameters has the effect of introducing some bias error into the model, but by removing these parameters from the estimated set, we improve the reliability with which the remaining parameters are estimated.

Subset selection is most powerful if the eigenvalue spectrum of the Hessian matrix exhibits a large gap between $\rho$ large eigenvalues and $m - \rho$ small ones. Such a situation suggests that the Hessian matrix has numerical rank $\rho$ and that $m - \rho$ appropriately chosen parameters should be fixed. Equations (2.4) and (2.5) then only involve reduced-order Hessian and Jacobian matrices, which we will denote by $\mathbf{H}_\rho$ and $\mathbf{J}_\rho$, respectively.

The following subset selection algorithm for non-linear least squares estimation is based on the work of Vélez-Reyes [45] and is essentially an extension of a subset selection algorithm for the linear least squares problem [13, 14]:

1. Given an initial estimate $\theta_0$, compute the Hessian $\mathbf{H}(\theta_0)$ and its eigenvalue decomposition $\mathbf{H} = \mathbf{V}\Lambda\mathbf{V}^\mathsf{T}$.
2. Determine $\rho$ and an ordering of the eigenvalues in the decomposition such that the first $\rho$ eigenvalues of $\mathbf{H}$ are much larger than the remaining $m - \rho$.
3. Partition the matrix of eigenvectors according to $\mathbf{V} = [\mathbf{V}_\rho \;\; \mathbf{V}_{m-\rho}]$.
4. Determine a permutation matrix $\mathbf{P}$ by constructing a QR decomposition with column pivoting [14, p. 248] for $\mathbf{V}_\rho^\mathsf{T}$, i.e., determine $\mathbf{P}$ such that

$$\mathbf{V}_\rho^\mathsf{T} \cdot \mathbf{P} = \mathbf{Q} \cdot \mathbf{R},$$

where $\mathbf{Q}$ is an orthogonal matrix and the first $\rho$ columns of $\mathbf{R}$ form an upper triangular matrix.

5. Use $\mathbf{P}$ to re-order the parameter vector $\theta$ according to $\tilde{\theta} = \mathbf{P}^{\mathsf{T}}\theta$.
6. Make the partition $\tilde{\theta} = [\tilde{\theta}_{\rho}^{\mathsf{T}} \;\; \tilde{\theta}_{m-\rho}^{\mathsf{T}}]^{\mathsf{T}}$, where $\tilde{\theta}_{\rho}^{\mathsf{T}}$ contains the first $\rho$ elements of $\tilde{\theta}$. Fix $\tilde{\theta}_{m-\rho}$ at a prior estimate $\hat{\tilde{\theta}}_{m-\rho}$.
7. Compute the new estimate of the parameter vector $\hat{\tilde{\theta}}$ by solving the reduced-order minimization problem

$$\hat{\tilde{\theta}} = \arg\min_{\tilde{\theta}} \Phi(\tilde{\theta}) \quad \text{subject to} \quad \hat{\tilde{\theta}}_{m-\rho} = \tilde{\theta}_{m-\rho}.$$

The eigenvalue decomposition in the first step is a pre-requisite for the determination of the numerical rank of $\mathbf{H}$ and the subset selection step. The rank determination in step 2 is based on reasonably sized gaps in the eigenvalue spectrum. Such gaps might not exist, and in those cases subset selection might only be of limited help in overcoming ill-conditioning [13]. Usually several gaps of differing sizes can be identified and one has to choose between including more parameters and keeping the condition number of the reduced order Hessian $\mathbf{H}_{\rho}$ small. The former choice usually increases the reduced-order model's ability to represent experimental data, while the latter leads to more reliable estimation of the remaining parameters. The numerical rank estimate tells us how many parameters to include in our analysis. Step 4, the actual subset selection step, determines *which* parameters to include. This information is encoded in the permutation matrix $\mathbf{P}$. Step 5 reorders the parameter vector $\theta$ such that the $\rho$ dominant parameters move to the top of the vector. Steps 6 and 7 describe the reduced-order estimation step.

We applied the subset selection algorithm outlined above to the problem of estimating cardiovascular parameters from the transient hemodynamic response to standing up detailed in Sect. 2.2.

Figure 2.9 shows the eigenvalue spectrum $\{\lambda_i\}$ of the approximate Hessian matrix $\mathbf{H}(\theta_0) = \mathbf{J}^{\mathsf{T}}\mathbf{J}$. Since the spectrum covers almost eight orders of magnitude, we plot the eigenvalues on a logarithmic scale. The corresponding condition number of the full-order Hessian matrix is $\kappa(\mathbf{H}) = 3.4 \cdot 10^7$, indicating substantial ill-conditioning if attempts were made to solve the full-order estimation problem. Figure 2.9 also shows the gap structure $\{\lambda_i/\lambda_{i+1}\}$ of the eigenvalue spectrum. It is evident from the two figures that no single dominantly large gap exists that would suggest an obvious choice for the rank estimate. However, the gap structure does show three breakpoints that are sufficiently removed from the remainder of the spectrum. They correspond to the rank estimates $\rho_1 = 3$, $\rho_2 = 1$, and $\rho_3 = 4$, where $\rho_1$ corresponds to the largest gap, $\rho_2$ to the second largest and so on.

We compared the rank estimate $\rho = 4$ against an arbitrarily chosen one, $\rho = 15$, to demonstrate the effect of ill-conditioning on the parameter estimates. Table 2.1 shows the results of this exploration and demonstrates that including more parameters in the estimation scheme than warranted by the subset selection criterion yields unreliable estimates even for those parameters that by themselves might be identifiable. A more detailed discussion of the methodology, evaluation strategy, and results of subset selection in the context of cardiovascular parameter estimation can be found in [17].

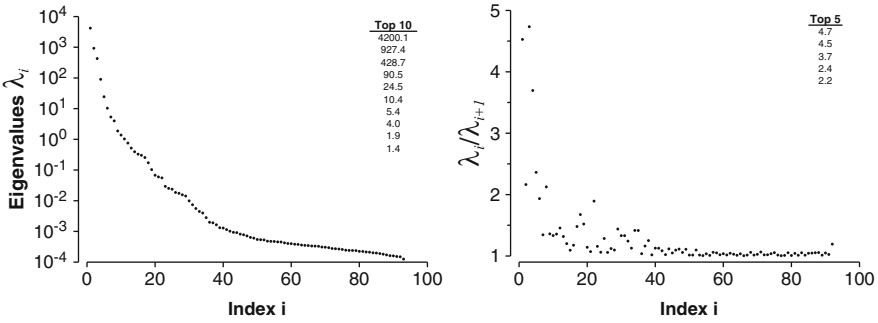


**Fig. 2.9** Eigenvalue spectrum of the Hessian matrix (*left*) and gaps $\lambda_i/\lambda_{i+1}$ of the eigenvalue spectrum

**Table 2.1** Mean relative errors of estimated parameters with respect to their true values. Numeric values are given in %. Parameters are: Setpoint of the arterial blood pressure (1), right-ventricular end-diastolic elastance (2), total blood volume (3), and nominal heart rate (4)

| | | Parameter index | | | |
|---|---|---|---|---|---|
| | $\kappa(\mathbf{H}_\rho)$ | 1 | 2 | 3 | 4 |
| $\rho = 4$ | 55.3 | (−0.9±0.3) | (0.1±0.2) | (0.4±0.1) | (0.7±0.4) |
| $\rho = 15$ | $8.0 \cdot 10^4$ | (−21.1±2.5) | (4.6±4.2) | (−5.6±1.2) | (32.1±6.8) |

## 2.5 The Case for Structured Model-Order Reduction

When developing physiological models, researchers commonly do not strive to build a minimal model capable of representing particular experimental observations. Rather, they usually represent all components of the physiological system that may contribute significantly to particular observations. Consequently, the resultant models can become quite sizable, representing physiology at a variety of time and space scales. Such models typically embody or reflect the underlying physical or mechanistic understanding we have about the system, as well as structural features such as the delineation of subsystems and their interconnections. Often, these models have been built up over decades of study and reflect the cumulative knowledge and contributions of many researchers in a field.

However, increasing the complexity of a model can significantly work against its usefulness in many respects, as simulation times are increased and it becomes difficult to understand in a fundamental way what parts of a model are actually being exercised and how. In addition, a significant feature of such models is the uncertainty associated with many or most of the parameters of the model. The data that one can collect from the associated physiological system is rarely rich enough to allow reliable identification of all model parameters (see Sect. 2.4), yet there are good reasons not to be satisfied with direct black-box identification of a reduced-order model [1]. The challenge then is to develop meaningful reduced-order models

that reflect the detailed, hard-won knowledge one has about the system, while being better suited to identification, simulation, and control design than the original large model. Currently, no such tools for *structured* or *gray-box* model-order reduction exist, though the need to develop such tools is quite obvious: only if we are able to identify those components of a model that contribute significantly to a particular simulated response do we actually increase our understanding of the system under study, and only if we are able to quantify the effects of parametric uncertainties can we assess the model's range of validity and can we suggest experiments that might help reduce prediction uncertainties.

## 2.6 Conclusions

Physiology has always been an integrative and quantitative science in which mathematical analyses and modeling featured very prominently alongside experimentation to illuminate experimental results and to test our understanding of physiology in an exact, quantitative framework. The need to continue in this tradition is ever more urgent as the recent explosion in biological, biomedical, and clinical data necessitates novel approaches to the integration, analysis, and interpretation of such overwhelmingly copious amounts of data. In this introductory chapter, we have touched upon some key themes of mathematical modeling, namely simulation, exploration of hypotheses, parameter estimation and model-order reduction. Many of the contributions in this volume elaborate on one or the other of these themes in their application of modeling in physiology or biology.

**Acknowledgements** This work was partially supported by the United States National Aeronautics and Space Administration through the Cooperative Agreement NCC-52 with the National Space Biomedical Research Institute, and through grant R01 001659 from the National Institute of Biomedical Imaging and Bioengineering of the US National Institutes of Health.

## References

1. Antoulas, A.: Approximation of Large-Scale Dynamical Systems. Advances in Design and Control. SIAM, Philadelphia, PA (2005)
2. Bard, Y.: Nonlinear Parameter Estimation. Academic, New York (1974)
3. Bassingthwaighte, J.: Strategies for the physiome project. Ann. Biomed. Eng. **28**, 1043–1058 (2000)
4. Boyers, D., Cuthbertson, J., Luetscher, J.: Simulation of the human cardiovascular system: A model with normal response to change in posture, blood loss, transfusion, and autonomic blockade. Simulation **18**, 197–205 (1972)
5. Brunberg, A., Heinke, S., Spillner, J., Autschbach, R., Abel, D., Leonhardt, S.: Modeling and simulation of the cardiovascular system: A review of applications, methods, and potentials. Biomed. Tech. (Berl.) **54**(5), 233–244 (2009)

6. Burth, M., Verghese, G., Vélez-Reyes, M.: Subset selection for improved parameter estimation in on-line identification of a synchronous generator. IEEE Trans. Power Syst. **14**(1), 218–225 (1999)
7. Consensus Committee of the American Autonomic Society and the American Academy of Neurology: Consensus statement on the definition of orthostatic hypotension, pure autonomic failure and multiple system atrophy. Clin. Auton. Res. **6**, 125–126 (1996)
8. Crampin, E., Halstead, M., Hunter, P., Nielsen, P., Noble, D., Smith, N., Tawhai, M.: Computational physiology and the physiome project. Exp. Physiol. **89**(1), 1–26 (2004)
9. Croston, R., Fitzjerrell, D.: Cardiovascular model for the simulation of exercise, lower body negative pressure, and tilt table experiments. Proceedings of the Fifth Annual Pittsburgh Conference on Modeling and Simulation, pp. 471–476 (1974)
10. Croston, R., Rummel, J., Kay, F.: Computer model of cardiovascular control system response to exercise. J. Dyn. Syst. Meas. Control **95**, 301–307 (1973)
11. Dickinson, C.: A digital computer model of the effects of gravitational stress upon the heart and venous system. Med. Biol. Eng. **7**, 267–275 (1969)
12. Frank, O.: Die Grundform des arteriellen Pulses. Erste Abhandlung. Mathematische Analyse. Z. Biol. **37**, 483–526 (1899)
13. Golub, G., Klema, V., Stewart, G.: Rank degeneracy and least squares problems. Technical Report TR-456, Department of Computer Science, University of Maryland, College Park, MD (1976)
14. Golub, G., van Loan, C.: Matrix Computations, 3rd edn. Johns Hopkins University Press, Baltimore, MD (1996)
15. Green, J., Miller, N.: A model describing the response of the circulatory sytem to acceleration stress. Ann. Biomed. Eng. **1**(4), 455–467 (1973)
16. Guyton, A., Coleman, T.: Quantitative analysis of the pathophysiology of hypertension. Circ. Res. **24**(Suppl. I), I1–I19 (1969)
17. Heldt, T.: Computational models of cardiovascular response to orthostatic stress. Doctoral dissertation, Harvard-MIT Division of Health Sciences and Technology, Massachusetts Institute of Technology, Cambridge, MA (2004). Http://dspace.mit.edu/handle/1721.1/28761
18. Heldt, T., Mark, R.: Scaling cardiovascular parameters for population simulations. Comput. Cardiol. **31**, 133–136 (2004). Available at http://www.cinc.org/archives/2004/133.pdf
19. Heldt, T., Mark, R.: Understanding post-spaceflight orthostatic intolerance – A simulation study. Comput. Cardiol. **32**, 631–634 (2005). Available at http://www.cinc.org/archives/2005/0631.pdf
20. Heldt, T., Mukkamala, R., Moody, G., Mark, R.: CVSim: An open-source cardiovascular simulator for teaching and research. Open Pacing Electrophysiol. Ther. J. **3**, 45–54 (2010)
21. Heldt, T., Oefinger, M., Hoshiyama, M., Mark, R.: Circulatory response to passive and active changes in posture. Comput. Cardiol. **29**, 263–266 (2003). Available at http://www.cinc.org/archives/2003/263.pdf
22. Heldt, T., Shim, E., Kamm, R., Mark, R.: Computational modeling of cardiovascular response to orthostatic stress. J. Appl. Physiol. **92**(3), 1239–1254 (2002)
23. Heldt, T., Verghese, G., Long, W., Szolovits, P., Mark, R.: Integrating data, models, and reasoning in critical care. In: Proceedings of the 28th IEEE EMBC International Conference, pp. 350–353. IEEE Engineering in Medicine and Biology Society (2006)
24. van Heusden, K., Gisolf, J., Stok, W., Dijkstra, S., Karemaker, J.: Mathematical modeling of gravitational effects on the circulation: Importance of the time course of venous pooling and blood volume changes in the lungs. Am. J. Physiol. **291**(5), H2152–H2165 (2006)
25. Hodgkin, A., Huxley, A.: A quantitative description of membrane current and its application to conduction and excitation in nerve. J. Physiol. **117**, 500–544 (1952)
26. Hunter, P., Borg, T.: Integration from proteins: The physiome project. Nat. Rev. Mol. Cell Biol. **4**, 237–243 (2003)
27. Jaron, D., Moore, T., Bai, J.: Cardiovascular response to acceleration stress: A computer simulation. Proc. IEEE **76**(6), 700–707 (1988)

28. Jaron, D., Moore, T., Chu, C.L.: A cardiovascular model for studying impairment of cerebral function during +Gz stress. Aviat. Space Environ. Med. **55**(1), 24–31 (1984)
29. Leonard, J., Leach, C., Rummel, J.: Computer simulations of postural change, water immersion, and bedrest: An integrative approach for understanding the spaceflight response. Physiologist **22**(6), S31–S32 (1979)
30. Meck, J., Waters, W., Ziegler, M., deBlock, H., Mills, P., Robertson, D., Huang, P.: Mechanisms of post-spaceflight orthostatic hypotension: $\alpha_1$-adrenergic receptor responses before flight and central autonomic dysregulation post-flight. Am. J. Physiol. **286**(4), H1486–H1495 (2004)
31. Melchior, F., Srinivasan, R., Clère, J.: Mathematical modeling of the human response to LBNP. Physiologist **35**(1 Suppl.), S204–S205 (1992)
32. Melchior, F., Srinivasan, R., Thullier, P., Clère, J.: Simulation of cardiovascular response to lower body negative pressure from 0 to −40 mmHg. J. Appl. Physiol. **77**(2), 630–640 (1994)
33. Noble, D.: The surprising heart: A review of recent progress in cardiac electrophysiology. J. Physiol. **353**, 1–50 (1984)
34. Olufsen, M., Ottesen, J., Tran, H., Ellwein, L., Lipsitz, L., Novak, V.: Blood pressure and blood flow variation during postural change from sitting to standing: Model development and validation. J. Appl. Physiol. **99**(4), 1523–1537 (2005)
35. Peterson, K., Ozawa, E., Pantalos, G., Sharp, M.: Numerical simulation of the influence of gravity and posture on cardiac performance. Ann. Biomed. Eng. **30**(2), 247–259 (2002)
36. Platts, S., Ziegler, M., Waters, W., Mitchell, B., Meck, J.: Midodrine prescribed to improve recurrent post-spaceflight orthostatic hypotension. Aviat. Space Environ. Med. **75**(6), 554–556 (2004)
37. Ramsdell, C., Mullen, T., G.H., S., Rostoft, S., Sheynberg, N., Aljuri, N., Maa M. amd Mukkamala, R., Sherman, D., Toska, K., Yelle, J., Bloomfield, D., Williams, G., Cohen, R.: Midodrine prevents orthostatic intolerance associated with simulated microgravity. J. Appl. Physiol. **90**(6), 2245–2248 (2001)
38. Simanonok, K., Srinivasan R.S. Myrick, E., Blomkalns, A., Charles, J.: A comprehensive guyton model analysis of physiologic responses to preadapting the blood volume as a countermeasure to fluid shifts. J. Clin. Pharmacol. **34**(5), 440–453 (1994)
39. Simanonok, K., Srinivasan, R., Charles, J.: A computer simulation study of preadaptation of the circulation by removal of different blood volumes to counteract fluid shifts. Physiologist **35**(1 Suppl.), S111–S112 (1992)
40. Smith, J., Hughes, C., Ptacin, M., Barney, J., Tristani, F., Ebert, T.J.: The effect of age on hemodynamic response to graded postural stress in normal men. J. Gerontol. **42**(4), 406–411 (1987)
41. Snyder, M., Rideout, V.: Computer simulation studies of the venous circulation. IEEE Trans. Biomed. Eng. **BME-16**(4), 325–334 (1969)
42. Srinivasan, R., Simanonok, K., Charles, J.: Computer simulation analysis of the effects of countermeasures for reentry orthostatic intolerance. Physiologist **35**(1 Suppl.), S165–S168 (1992)
43. Sud, V., Srinivasan, R., Charles, J., Bungo, M.: Effects of lower body negative pressure on blood flow with applications to the human cardiovascular system. Med. Biol. Eng. Comput. **31**(6), 569–575 (1993)
44. Summers, R., Martin, D., Meck, J., Coleman, T.: Computer systems analysis of spaceflight induced changes in left ventricular mass. Comput. Biol. Med. **37**(3), 358–363 (2007)
45. Vélez-Reyes, M.: Decomposed algorithms for parameter estimation. Doctoral dissertation, Massachusetts Institute of Technology, Cambridge, MA (1992)
46. Vogel, C.: Computational Methods for Inverse Problems. Frontiers in Applied Mathematics. SIAM, Philadelphia (2002)
47. Waters, W., Ziegler, M., Meck, J.: Postspaceflight orthostatic hypotension occurs mostly in women and is predicted by low vascular resistance. J. Appl. Physiol. **2**(92), 596–594 (2002)
48. White, R., Blomqvist, C.: Central venous pressure and cardiac function during spaceflight. J. Appl. Physiol. **85**(2), 738–746 (1998)

49. White, R., Fitzjerrell, D., Croston, R.: Cardiovascular modelling: Simulating the human response to exercise, lower body negative pressure, zero gravity and clinical conditions. In: Advances in Cardiovascular Physics, vol. 5 (Part 1), pp. 195–229. Karger, Basel (1983)
50. White, R., Fitzjerrell, D., Croston, R.: Fundamentals of lumped compartmental modelling of the cardiovascular system. In: Advances in Cardiovascular Physics, vol. 5 (Part 1), pp. 162–184. Karger, Basel (1983)
51. White, R., Leonard, J., Srinivasan, R., Charles, J.: Mathematical modeling of acute and chronic cardiovascular changes during extended duration orbiter (EDO) flights. Acta Astronaut. **23**, 41–51 (1991)
52. Zamanian, A.: Modeling and simulating the human cardiovascular response to acceleration. SM thesis, Department of Electrical Engineering and Computer Science, Massachusetts Institute of Technology, Cambridge, MA (2007)